

1 Inferring the Photolysis Rate of NO₂ in the Stratosphere

2 Based on Satellite Observations

3 Jian Guan¹, Susan Solomon¹, Sasha Madronich^{2,3}, Douglas Kinnison²

4 ¹Department of Earth, Atmospheric, and Planetary Sciences, MIT; Cambridge, MA, 02139, USA

5 ²Atmospheric Chemistry Observations and Modeling Laboratory, National Center for Atmospheric Research, Boulder,
6 CO, 80301, USA

7 ³USDA UV-B Monitoring and Research Program, Natural Resource Ecology Laboratory Colorado State University, Fort
8 Collins, Colorado, 80523, USA

9 Correspondence to: Jian Guan (jianguan@mit.edu)

10 **Abstract.** NO and NO₂ (NO_x) play major roles in both tropospheric and stratospheric chemistry. This paper provides a novel
11 method to obtain a global and accurate photodissociation coefficient for NO₂ based on satellite data. The photodissociation
12 coefficient J_{NO₂} dominates the daytime diurnal variation of NO_x photochemistry. Here the spatial variation of J_{NO₂} in 50° S-90° S
13 in December from 20-40 km is obtained using data from the Michelson Interferometer for Passive Atmospheric Sounding (MIPAS)
14 experiment. Because NO and NO₂ exchange rapidly with one another in the daytime, the J_{NO₂} can be attained assuming steady
15 state, and the results are shown to be consistent with model results. The J_{NO₂} value decreases as the solar zenith angle increases
16 and has a weak altitude dependence. A key finding is that the satellite-derived J_{NO₂} increases in the polar regions in good agreement
17 with model predictions, due to the effects of ice and snow on surface albedo. Thus, the method presented here provides an
18 observations-based check on the role of albedo in driving polar photochemistry.

19 1 Introduction

20 Fast photochemistry in the Earth's atmosphere is driven by sunlight and affects the diurnal variation of many species. The properties
21 of sunlight entering the stratosphere, including light intensity and its energy distribution, depend on the solar zenith angle, as well
22 as ~~distributions of absorbing species~~. Further, the solar zenith angle is related to latitude, season, and local time. The sunlight
23 entering the stratosphere determines the photochemical rates in the stratosphere, thus affecting stratospheric chemistry, and the
24 diurnal variations of species concentration is one of the impacts. Therefore, diurnal variation observations provide key information
25 in analyzing the photochemical properties of the stratosphere. NO_x chemistry is one of the most important elements of stratospheric
26 chemistry and plays a leading role in controlling stratospheric ozone concentration (Crutzen, 1979; Johnston, 1971; Crutzen, 1970).
27 The photodissociation coefficient J_{NO₂} quantifies the process of NO₂ photolysis into NO, thus affecting the diurnal variation of
28 NO_x. The stratospheric NO and NO₂ abundances are controlled by the following reactions:



33 Because of the short lifetime of NO and NO₂, they are in steady state within the sunlit stratosphere. Therefore, the following
34 equation holds:

35
$$\frac{[\text{NO}]}{[\text{NO}_2]} \approx \frac{J_{\text{NO}_2} + k_{\text{O} + \text{NO}_2} \times [\text{O}]}{(k_{\text{NO} + \text{O}_3} \times [\text{O}_3] + k_{\text{NO} + \text{ClO}} \times [\text{ClO}])}$$
 (1)

Deleted: the overhead concentrations of oxygen and ozone and the reflective properties of the underlying troposphere

Deleted: v

39 A number of studies on the diurnal variation of NOx and J_{NO_2} in the stratosphere have been reported, based on models or airborne
40 observations. Fabian et al. (1982) used a two-dimensional model to examine the diurnal variations of NOx at different altitudes.
41 Many studies focused on the diurnal variation of NOx using airborne observations, and these were subsequently compared with
42 models. (Pommereau, 1982; Roscoe et al., 1986; Kawa et al., 1990). Madronich et al. (1985) measured J_{NO_2} in the stratosphere
43 utilizing a balloon platform and compared it to a model; they showed that the J_{NO_2} value has a weak altitude dependence. Webster
44 and May (1987) measured the diurnal variation of NOx and J_{NO_2} simultaneously utilizing a balloon. Del Negro et al. (1999)
45 calculated J_{NO_2} based on the concentrations of NO, NO₂, O₃, ClO, and HO₂ measured on an aircraft and BrO from a model, and
46 compared them with a model. They found that the J_{NO_2} inferred from the data assuming steady state matched their model well.
47 Moreover, it has been emphasized that albedo has a substantial effect on J_{NO_2} (Madronich, 1987; Bösch et al., 2001; Laepple, 2005;
48 Walker et al., 2022). Further, the surface albedo over ice and snow has a large and important effect on tropospheric chemistry in
49 the polar regions (Walker et al., 2022) due in large part to its effect on J_{NO_2} , highlighting the need to evaluate J_{NO_2} on a large scale.
50 Surface radiometers have also been used to infer information about J_{NO_2} for different sky conditions in the troposphere (Shetter et
51 al., 1992; Junkermann et al., 1989). However, aircraft, surface radiometers, or balloon measurements are all local and the amount
52 of data is therefore limited. At the same time, models are based on theoretical calculations and require measured data for verification.
53 These considerations are the motivation for this paper, in which satellite data are used to characterize J_{NO_2} on a global basis, with
54 particular emphasis on values obtained over ice and snow.

55 Satellite measurements of NOx allow elucidation of its zenith angle and albedo dependence. The global concentrations of NO,
56 NO₂, and related species as discussed below can be easily obtained using satellite data and used to determine J_{NO_2} at different
57 latitudes, albedo, and altitudes. Solomon et al. (1986) reported satellite observations of the NO₂ diurnal variation in the stratosphere
58 at solar zenith angles ranging from about 35 to 110 degrees but concurrent NO data were not available. Anderson et al. (1981)
59 employed a similar method to study the zenith angle variation of mesospheric O₃. The Michelson Interferometer for Passive
60 Atmospheric Sounding (MIPAS) is a Fourier transform spectrometer carried on Envisat, measuring not only NO₂ but also NO and
61 O₃, as well as ClO, all of which are used here in inferring J_{NO_2} (see below). MIPAS was designed and operated for the measurement
62 of atmospheric species from space and can detect limb emission in the middle atmosphere with high spectral resolution and low-
63 noise performance (Fischer et al., 2008).

64 In this work, the novel method of obtaining the zenith angle dependence of NOx and J_{NO_2} using satellite data in summer over the
65 polar cap is reported, taking 50° S-90° S in December in 20-40 km as an example. The diurnal variations of NOx and J_{NO_2} at
66 different altitudes are described. J_{NO_2} changes with latitude are discussed and a J_{NO_2} map in the Antarctic is used to elucidate
67 albedo effects. In summary, this work shows a method for obtaining NOx diurnal variation and accurate J_{NO_2} based on satellite
68 data, expanding the way to attain information on this key photodissociation coefficient.

69 2 Data and Methods

70 2.1 MIPAS Data

71 The vertical resolution of MIPAS is approximately 3-8 km in the stratosphere, and the horizontal resolution is 30 km across track,
72 about 500 km for along-track until 2004 (400 km after 2004). The vertical scan range is 5-150 km. Satellite operation was stopped
73 temporarily in March 2004 due to technical issues and resumed in January 2005 in a new operation mode. MIPAS allows near
74 complete global coverage, ranging from 87° S to 89° N obtained about every three days by 73 scans per orbit and 14.3 orbits per
75 day. Each day the satellite passes through the same latitude at two local times (ascending side and descending side, as shown in

Deleted: Many studies of the NOx diurnal variation based on airborne observations which were then compared with models ...

Deleted: backscatter

Deleted: of MIPAS

Deleted: ,

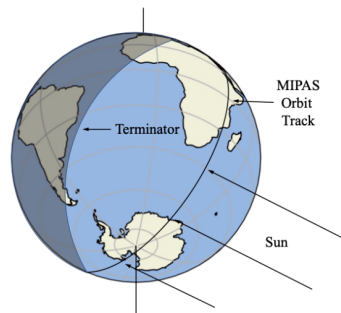
Deleted: and t

83 Fig. 1). Therefore, for this dataset, there are only two solar zenith angles at each latitude. We therefore focus on 50° S-90° S in the
84 polar day, in December 2009, where there are as many solar zenith angles as possible in a relatively small latitude range. The data
85 from the satellite was averaged daily and zonally (Because the specific latitudes of the satellite data vary somewhat from one orbit
86 to another, we bin the data using a two-degree interval). Then we calculate the four-day running mean, which is shown in Fig. 2
87 and Fig. 3.

88 In this paper, we used the NO, NO₂, O₃, ClO, temperature and pressure data from V8 MIPAS retrievals performed with the
89 IMK/IAA level 2 processor. The retrieval of temperature was reported by Kiefer et al. (2021). For NO retrieval, the method
90 considered the populations of excited NO states (Funke et al., 2005). This implies that photolysis of NO₂ is included in the retrieval
91 priors. However, retrieved NO is only weakly dependent on prior knowledge of J_{NO₂} values (10-15%). In our calculations,
92 according to Eq. (2) and (3), NO, NO₂ and O₃ play comparable roles in calculation of J_{NO₂}, reducing the impact of prior knowledge
93 on the final results. Therefore, prior knowledge of J_{NO₂} will have a small effect on our findings as long as prior knowledge of J_{NO₂}
94 is not completely incorrect. The NO retrieval was documented by Funke et al. (2023). These authors reported an accuracy of 8-
95 15% for altitudes of 20 to 40 km. Regarding O₃, Kiefer et al. (2023) reported an accuracy of 3-8% in the altitude region of interest.
96 The retrievals of NO₂ and ClO were described by Funke et al. (2005) and von Clarmann et al. (2009), respectively, with accuracies
97 of 0.2-0.8 ppbv for NO₂ and total error of more than 35% for ClO. However, please note that these papers refer to older data
98 versions. Accuracy estimates for V8 ClO and NO₂ are not yet available but the values quoted here were used as a rough guideline.

Deleted: were

Deleted: from V8 level 2 MIPAS retrievals. The reported precision between 20 km and 40 km is 5-15 % for NO, 5-15 % for NO₂, 2-3 % for O₃ and more than 35 % for ClO.



99
100 Figure 1. Schematic representation of the MIPAS orbit at high latitude in December showing the ascending (dayside) and
101 descending (nightside) portions of the orbit and the terminator.

102 2.2 Model Calculations

103 The Whole Atmosphere Community Climate Model version 6 (WACCM6) is used in this study. WACCM6 is a component of the
104 Community Earth System Model version 2 (CESM2; Gettelman et al., 2019; Danabasoglu et al., 2020). The horizontal resolution
105 is 1.9° latitude × 2.5° longitude and the with 88 vertical levels up to about 140 km, with the altitude resolution increasing from 0.1
106 km near the surface to 1.0 km in the upper troposphere–lower stratosphere (UTLS) and 1–2 km in the stratosphere. This work uses
107 the specified dynamics version of WACCM6, where the atmosphere below 50 km is nudged to the Modern-Era Retrospective
108 Analysis for Research and Applications, version 2 (MERRA-2; Gelaro et al., 2017), temperature and wind fields with a relaxation
109 time of 50 h. The chemistry mechanism includes a detailed representation of the middle atmosphere, with a sophisticated suite of
110 gas-phase and heterogeneous chemistry reactions, including the Ox, NOx, HOx, ClOx, and BrOx reaction families. There are ~100
111 chemical species and ~300 chemical reactions. Reaction rates are updated following Jet Propulsion Laboratory (JPL) 2015

116 recommendations (Burkholder et al., 2015). The photolytic approach is based on both inline chemical modules (<200nm) and a
117 lookup table approach (>200-750nm; see Kinnison et al., 2007). The look-up table (LUT) approach uses the Tropospheric
118 Ultraviolet-Visible Radiation Model (TUV4.2; Madronich, 1987; Madronich and Weller, 1990), an advanced radiation transfer
119 model widely used by the scientific community, using the four-stream pseudospherical discrete ordinates option. [TUV has](#)
120 [demonstrated excellent performance in intercomparisons with ground-based measurements, particularly under highly favorable](#)
121 [sky conditions \(Shetter et al., 2003\)](#). Model values for December 2009 at the same times and location as the satellite data are
122 selected by the [satellite profile algorithm](#) to compare with the satellite data, and denoted “Model”. [The satellite profile algorithm](#)
123 [outputs constituents \(e.g., J_{NO₂} and NO_x concentrations\) at the nearest latitude, longitude, and local time to the observation.](#)

124 2.3 Chemical Equation

125 NO is assumed to be in a steady state in the sunlit atmosphere at 20-40 km at least for zenith angles less than 94°, due to its short
126 lifetime. Using the chemistry discussed above, J_{NO₂} can then be expressed as

$$127 J_{NO_2} = \frac{[NO]}{[NO_2]} \times (k_{NO+O_3} \times [O_3] + k_{NO+ClO} \times [ClO]) - k_{O+NO_2} \times [O] \quad (2)$$

128 Where k is the rate constant, J_{NO₂} is the photodissociation coefficient of NO₂, and [O₃] is the concentration of O₃.

129 To obtain the concentration of O, O is assumed to be in a steady state with ozone at 20-40 km. The concentration of O can be
130 expressed as

$$131 [O] = \frac{J_{O_3} \times [O_3]}{k_{O+O_2+M} \times [O_2] \times [M]} \quad (3)$$

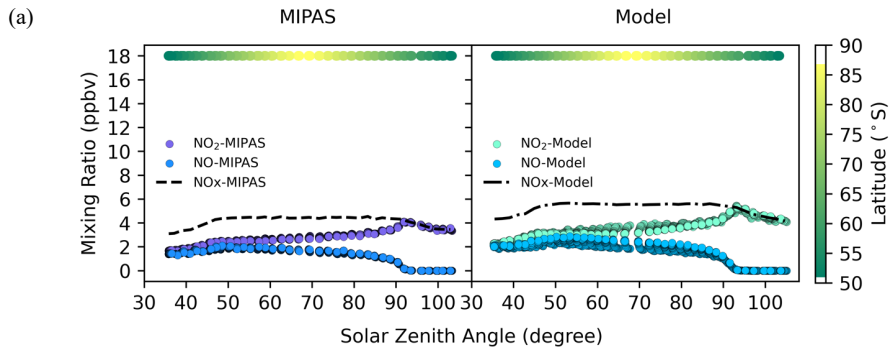
132 [The k_{NO+O₃}, k_{NO+ClO}, k_{O+NO₂} and their uncertainties are from JPL \(Burkholder et al., 2015\), and k_{O+O_{2+M}} and its uncertainty](#)
133 [are from International Union of Pure and Applied Chemistry \(IUPAC; Atkinson et al., 2004\)](#). It is worth noting that J_{O₃} in the Eq.
134 (3) comes from the model here, which is a limitation of this study. However, in the stratosphere below about 33 km [O] has a small
135 effect on J_{NO₂} [calculation](#) (less than 8.1 percent) [due to its low concentration \(Johnston and Podolske, 1978\)](#). ClO can similarly be
136 ignored when altitudes are less than 35 km, where ClO concentrations are small ([Sagawa et al., 2013](#)); otherwise using ClO data
137 from MIPAS would introduce large and unnecessary uncertainty. HO₂ and BrO both can react with NO but they are not measured
138 by MIPAS and their contributions to the partitioning between NO and NO₂ are negligibly small at the altitudes considered here
139 ([Del Negro et al., 1999](#)). Therefore, we don't consider them in this paper.

140 3 Results and Discussion

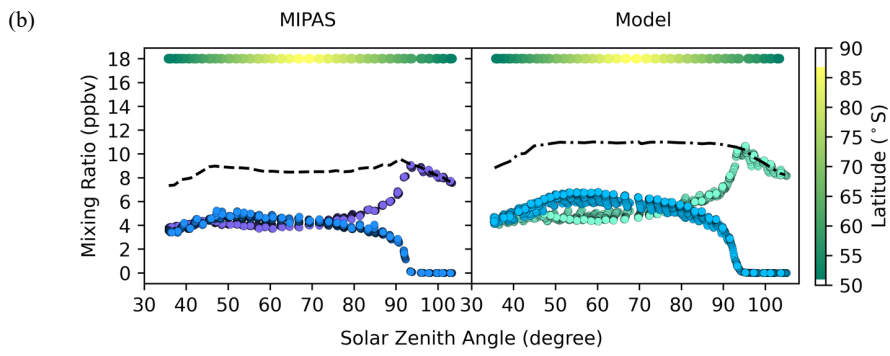
141 3.1 NO_x Concentration at different altitudes

142 To better understand the diurnal variation of NO_x, concentrations of NO and NO₂ from MIPAS and the model are shown in Fig.
143 2 at different altitudes. The NO and NO₂ concentrations from MIPAS and the model show very good overall consistency. The
144 solar zenith angle of 90 degrees is a clear dividing line, showing that light drives the diurnal variation, and the results are in good
145 accord with the theory.

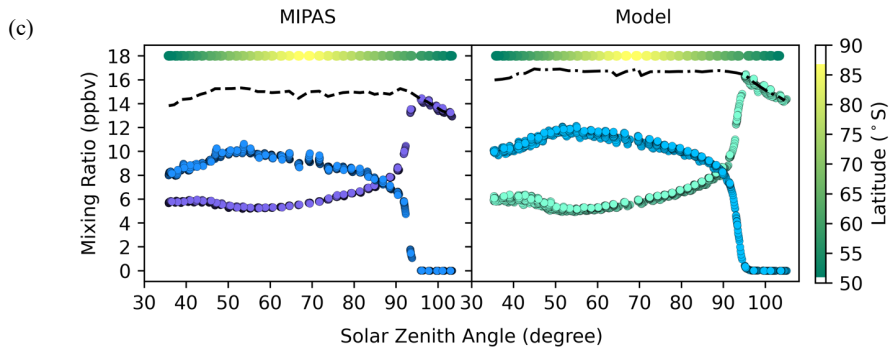
Deleted: a



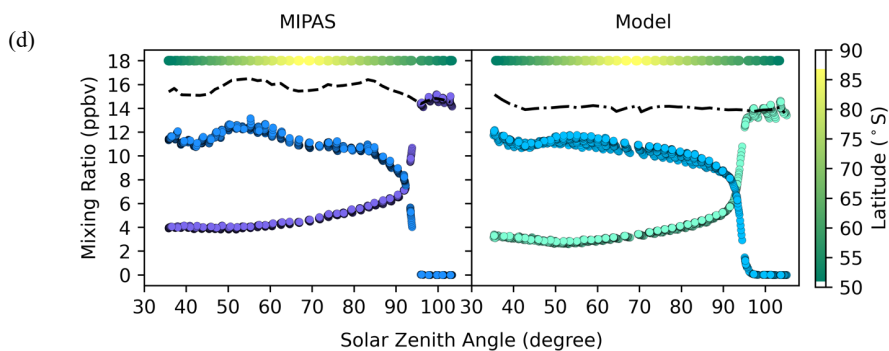
147



148



149



150

151 Figure 2. The concentrations of NO, NO₂ and NO_x in 50° S-90° S in December 2009 from MIPAS and the model at different
 152 altitudes. (a) 23 km (b) 28 km (c) 33 km (d) 38km. Model values are at the same time and location as the satellite data. The color
 153 bar represents the latitude of the data points at each solar zenith angle. **To ensure clear visual distinction for each point, black
 154 outlines are applied around them.**

155

156

157 NO and NO₂ exchange with one another but their sum (NO_x) varies relatively little for solar zenith angles less than about 90°. An
 158 increase in NO is matched by a decrease in NO₂ for zenith angles from about 30-50°, and then **NO concentration** decreases at
 159 larger angles, mainly reflecting changes in the photolysis rate as the satellite sweeps across the mid-latitudes and polar cap (see
 160 below). NO rapidly disappears when the solar zenith angle exceeds 90 degrees, **and the concentrations of NO and NO₂ change**
 161 **dramatically during twilight. NO decreases rapidly while NO₂ increases rapidly. When the solar zenith angle is more than 90**
 162 **degrees at these altitudes, NO is completely oxidized to NO₂, so there is no NO and NO₂/NO_x is 1. In addition, the concentration**
 163 **of NO₂ decreases slightly when the solar zenith angle is more than 90 degrees, which indicates the formation of the N₂O₃.**

164 It should also be noted that in Fig. 2, the concentrations of NO and NO₂ also reflect latitude variations, because the data at each
 165 zenith angle come from different latitudes as shown by the color bar at the top of each panel in Fig. 2, but these variations are fairly
 166 small over the summer polar cap and consistent with the model as shown. From 23 km to 33 km, the concentrations of NO and
 167 NO₂ increase with the altitude.

Deleted: Each point represents the four-day running mean of the average concentration of multiple daily measurements at two latitude degree intervals.

Deleted: so

Deleted: and

173 **3.2 J_{NO_2} at different altitudes and solar zenith angles**

174 Using Eq. (2) above, the J_{NO_2} and the error bar at different altitudes is shown in Fig. 3 along with the J_{NO_2} values from the model.
 175 The correlation diagrams show that the values inferred from the satellite observations are in excellent agreement with the model.
 176 Fig. 3 shows that the J_{NO_2} values at different altitudes within the 20–40 km range are nearly identical. This indicates the weak
 177 dependence of J_{NO_2} value on altitude, which was also reported by Madronich et al. (1985). This is because the NO_2 photolysis is
 178 largely driven by wavelengths ranging from 300 nm to 420nm (Madronich et al., 1983), which lie within a spectral region relatively
 179 free of atmospheric absorption. Consequently, the flux remains nearly constant at different altitudes. When the solar zenith angle
 180 is higher than about 90 degrees, the J_{NO_2} value drops rapidly to 0. The uncertainty is also shown in Fig. 3, and the model J_{NO_2} is
 181 within the error bar. The deviation between the results and model is significantly smaller than the 1- σ uncertainty, implying that
 182 the estimates of measurement errors of MIPAS may be conservative. To illustrate how different species affect our calculations at
 183 some altitudes, the effects of different gases at 38 km are shown in Fig. S1. The figure shows that O_3 , O and ClO are critical to
 184 NO_x chemistry at 38 km. However, the concentrations of ClO and O are smaller at altitudes of less than 35 km, and have about
 185 3.6% and less than 12% influence in our calculations, respectively. Moreover, the satellite data error of ClO becomes larger at
 186 lower altitudes, so ClO is not considered here when the altitude is lower than 35km.
 187

Deleted: calculated

Deleted: from 20–40 km,

Deleted: are nearly the same

Deleted: .

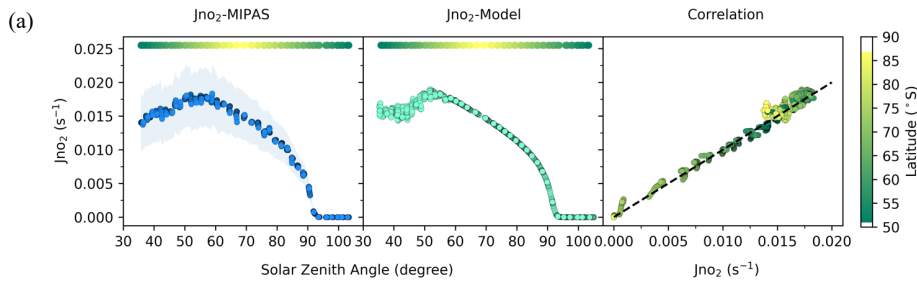
Deleted: This

Deleted: spectral region is

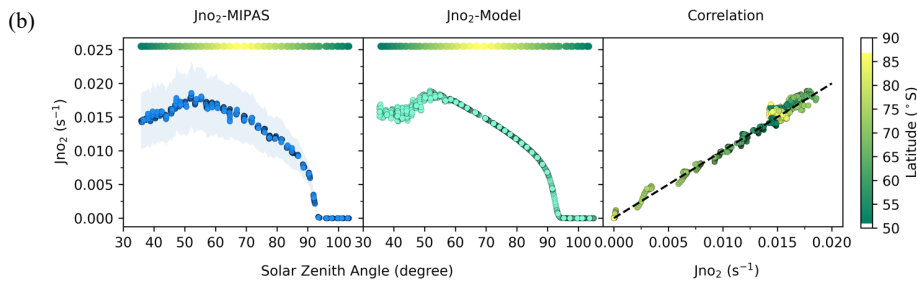
Deleted: , so the flux is nearly the same

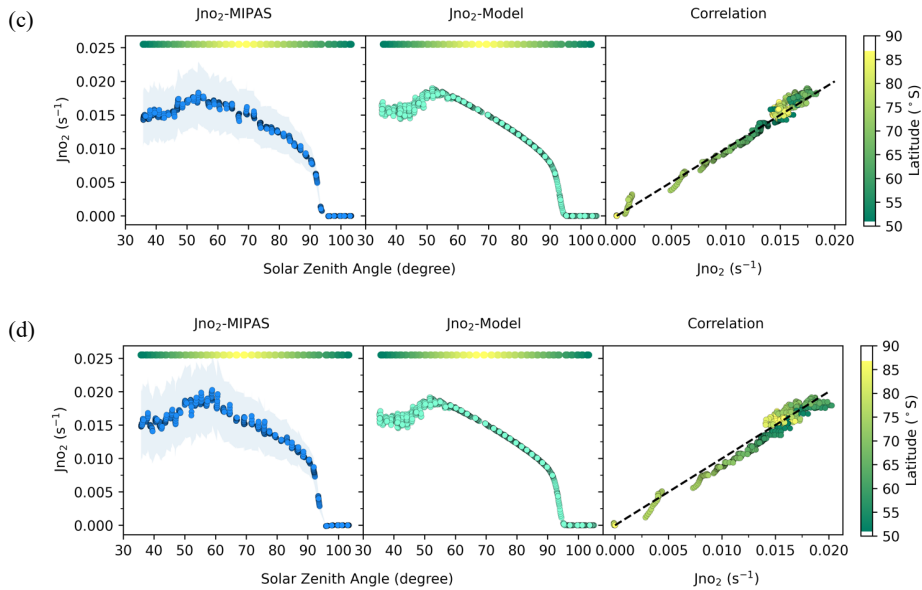
Deleted: levels

188



189





198

199

200

201

202

203

204

205

206

207

208

209

210

211

212

213

214

215

216

217

218

Figure 3. The J_{NO_2} in 50° S-90° S from MIPAS and the model at different altitudes. (a) 23 km (b) 28 km (c) 33 km (d) 38km. Model values are for the same time and location as the satellite data. The color bar represents the latitude of the data points at each solar zenith angle. In the correlation plots, the abscissa is J_{NO_2} -MIPAS and the ordinate is the J_{NO_2} -Model and the slope of dashed line is 1. To ensure clear visual distinction for each point, black outlines are applied around them.

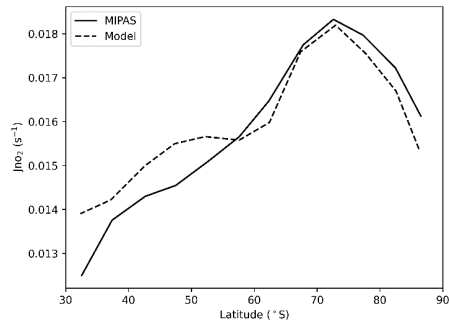
Deleted: The color bar represents the latitude of the data points at nearly the same solar zenith angle. Each point in J_{NO_2} -Model and J_{NO_2} -MIPAS represents the four-day running mean of the average J_{NO_2} of multiple daily measurements at two latitude degree intervals.

3.3 J_{NO_2} at different latitudes

The J_{NO_2} values from the satellite and model at different latitudes are next discussed. The clear relationship between J_{NO_2} and latitude from MIPAS and model is also displayed in Fig. 4, and the close comparison between the two is remarkable. It is obvious that the satellite-inferred J_{NO_2} monotonically increases with latitude from 30° S-70° S, and then decreases at higher latitudes. The J_{NO_2} over the pole is taken at a larger solar zenith angle, which explains its decrease relative to surrounding parts of Antarctica. Fig. 5 displays maps of the detailed distributions of J_{NO_2} from MIPAS and model, which exhibits their excellent consistency and shows a sharp transition between mid-latitudes and the Antarctic continent or regions covered by sea ice. The sharp transitions in J_{NO_2} values shown in Fig. 5 can only be caused by the large difference in albedo between the ocean and the Antarctic environs, covered by sea ice, land ice, and snow (Brandt et al., 2005; Shao and Ke, 2015). Albedo has a strong influence on J_{NO_2} because NO_2 is more sensitive than most atmospheric species to the effects of scattering and reflection (Madronich et al., 1983; Madronich, 1987; Bösch et al., 2001; Laepple et al., 2005). This is because the atmosphere exhibits considerable transparency at frequencies relevant to NO_2 photolysis, allowing a large number of photons to persist throughout the long atmospheric path, reaching Earth's surface and eventually returning to the stratosphere. In the high latitude area, the ground is covered with ice and snow, and the albedo can be as high as 0.9, while in the lower latitudes, the albedo is about 0.1 (Brandt et al., 2005; Shao and Ke, 2015). Table 1 shows the J_{NO_2} values at different solar zenith angles under different albedos. The results

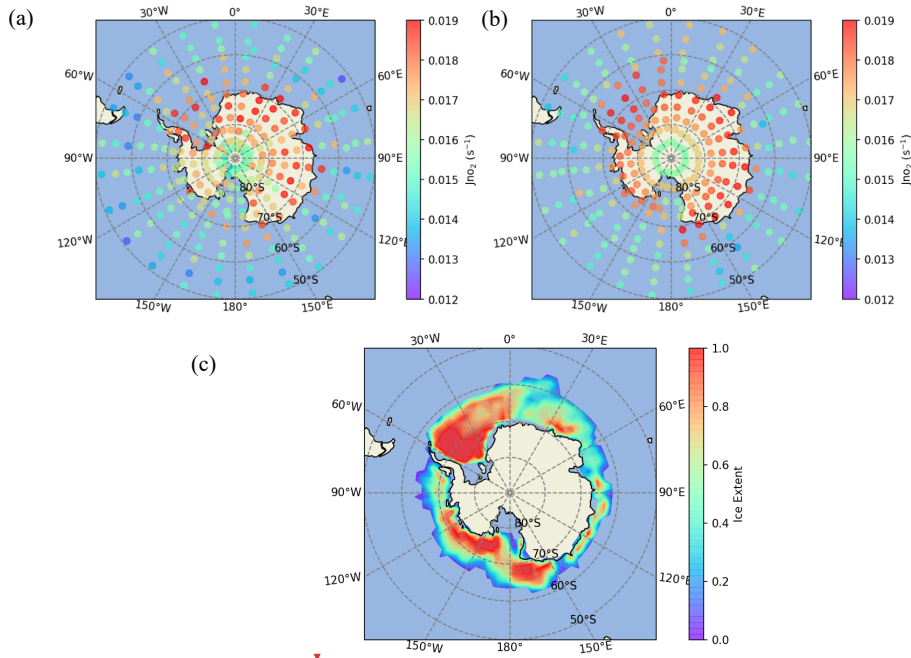
224 show that the albedo has a strong influence on the values, especially at low solar zenith angles. Based on Fig. 5, the J_{NO_2} above the
 225 continental ice is greater than that above the Antarctic sea ice, which may be because the fraction of open water within the pack
 226 influences the albedo (Brandt et al., 2005).

227
 228
 229



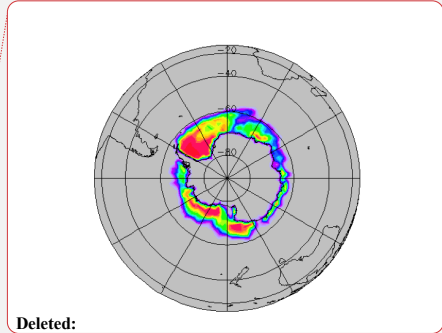
230
 231 Figure 4. The relationship between J_{NO_2} and latitude from MIPAS and model in 30° S-90° S at 28 km. Model data is for the same
 232 time and location as the satellite data. J_{NO_2} is examined wherever the solar zenith angle is less than 70 degrees and averaged
 233 every five degrees of latitude.

Deleted: arc



234

235



Deleted:

238 Figure 5. The mapping of J_{NO_2} in 50° S-90° S at 28 km from (a) MIPAS and (b) model. (c) The distribution of the sea ice extent
 239 in December 2009 in Antarctica from the model. Model J_{NO_2} data are for the same time and location as the satellite data. J_{NO_2} is
 240 shown wherever the solar zenith angle is less than 70 degrees and averaged every 3.33° latitude × 15° longitude.

Deleted: ,
 Deleted: and its albedo,

241
 242

Table 1. J_{NO_2} at different solar zenith angles under different albedos (α)

Solar zenith angle	J_{NO_2} ($\alpha = 0.1$)	J_{NO_2} ($\alpha = 0.9$)	J_{NO_2} ($\alpha = 0.9$)/ J_{NO_2} ($\alpha = 0.1$)
0	1.30	2.21	1.70
10	1.30	2.19	1.69
20	1.29	2.14	1.65
30	1.28	2.05	1.59
40	1.27	1.92	1.52
50	1.24	1.77	1.42
60	1.20	1.58	1.31
70	1.14	1.36	1.20
80	1.01	1.10	1.09
90	0.664	0.673	1.01

243

244 4 Conclusions

245 The diurnal variations of NO_x species and the resulting J_{NO_2} from about 50° S-90° S in December in 20-40 km have been evaluated
 246 based on MIPAS data. Light has a strong impact on the diurnal variations. NO and NO₂ are in steady state in the daytime and their
 247 sum is almost constant.

248 The calculated J_{NO_2} remarkably consistent with the model results, and the J_{NO_2} value decreases as the solar zenith angle increases.
 249 The J_{NO_2} value drops rapidly to 0 at the solar zenith angle of about 90 degrees. Moreover, the weak dependence of the J_{NO_2} value
 250 on altitude in this region is evident.

251 The results from the satellite and the model both indicate that J_{NO_2} increases with latitude, which can be attributed to more reflected
 252 light from ice and snow surfaces with high albedo. In summary, this work presents a new method for obtaining accurate J_{NO_2}
 253 values mainly based on satellite data. Further, this method can be extended to other photodissociation coefficients, paving the way
 254 for further tests of global photodissociation coefficients data based on satellites.

255

256 **Code and data availability.** The data and code are available at <https://doi.org/10.5281/zenodo.7764756>.

257 **Supplement.**

260 **Author contributions.** S.S. designed the study. J. G. analyzed the data and produced the figures. S. M. and D. K. run the models
261 and contributed significantly to the interpretation of findings. J.G. wrote the manuscript, with comments from all authors.

262 **Competing interests.** The contact author has declared that none of the authors has any competing interests.

263 **Disclaimer.** Publisher's note: Copernicus Publications remains neutral with regard to jurisdictional claims in published maps and
264 institutional affiliations.

265 **Acknowledgements.** Doug Kinnison was funded in part by NASA (grant no. 80NSSC19K0952). SS acknowledges support as the
266 Martin Professor of environmental studies at MIT, while JG appreciates an MIT presidential fellowship. SM acknowledges partial
267 support by the US Department of Agriculture (USDA) UV-B Monitoring and Research Program, Colorado State University, under
268 USDA National Institute of Food and Agriculture Grant 2019-34263-30552; 2022-34263-38472. The CESM project is supported
269 by the National Science Foundation and the Office of Science (BER) of the U.S. Department of Energy. We gratefully acknowledge
270 high-performance computing support from Cheyenne (doi:10.5065/D6RX99HX) provided by NCAR's Computational and
271 Information Systems Laboratory, sponsored by the National Science Foundation. We thank the Institute of Meteorology and
272 Climate Research - Atmospheric Trace Gases and Remote Sensing, and Dr. Michael Kiefer and Dr. Gabriele Stiller for MIPAS
273 data.

274

275 **References**

- 276 Anderson, G., Gille, J., Bailey, P., and Solomon, S.: LRIR observations of diurnal ozone variation in the mesosphere,
277 Quadrennial International Ozone Symposium, 580–585, 1981.
- 278 Atkinson, R., Baulch, D. L., Cox, R. A., Crowley, J. N., Hampson, R. F., Hynes, R. G., Jenkin, M. E., Rossi, M. J., and
279 Troe, J.: Evaluated kinetic and photochemical data for atmospheric chemistry: Volume I - gas phase reactions
280 of Ox, HOx, NOx and SOx species, *Atmos. Chem. Phys.*, 4, 1461–1738, [https://doi.org/10.5194/acp-4-1461-](https://doi.org/10.5194/acp-4-1461-2004)
281 2004, 2004.
- 282 Bösch, H., Camy-Peyret, C., Chipperfield, M., Fitzenberger, R., Harder, H., Schiller, C., Schneider, M., Trautmann, T.,
283 and Pfeilsticker, K.: Comparison of measured and modeled stratospheric UV/Visible actinic fluxes at large
284 solar zenith angles, *Geophys. Res. Lett.*, 28, 1179–1182, <https://doi.org/10.1029/2000GL012134>, 2001.
- 285 Brandt, R. E., Warren, S. G., Worby, A. P., and Grenfell, T. C.: Surface Albedo of the Antarctic Sea Ice Zone, *J. Climate*,
286 18, 3606–3622, <https://doi.org/10.1175/JCLI3489.1>, 2005.
- 287 Burkholder, J. B., Sander, S. P., Abbatt, J. P. D., Barker, J. R., Huie, R. E., Kolb, C. E., Kurylo, M. J., Orkin, V. L.,
288 Wilmouth, D. M., and Wine, P. H.: Chemical kinetics and photochemical data for use in atmospheric studies:
289 evaluation number 18, Pasadena, CA: Jet Propulsion Laboratory, National Aeronautics and Space
290 Administration, 2015.
- 291 Crutzen, P. J.: The influence of nitrogen oxides on the atmospheric ozone content, *Quarterly Journal of the Royal*
292 *Meteorological Society*, 96, 320–325, <https://doi.org/10.1002/qj.49709640815>, 1970.
- 293 Crutzen, P. J.: The Role of NO and NO₂ in the Chemistry of the Troposphere and Stratosphere, *Annu. Rev. Earth Planet.*
294 *Sci.*, 7, 443–472, <https://doi.org/10.1146/annurev.ea.07.050179.002303>, 1979.
- 295 Danabasoglu, G., Lamarque, J. -F., Baumeister, J., Bailey, D. A., DuVivier, A. K., Edwards, J., Emmons, L. K., Fasullo,
296 J., Garcia, R., Gettelman, A., Hannay, C., Holland, M. M., Large, W. G., Lauritzen, P. H., Lawrence, D. M.,

297 Lenaerts, J. T. M., Lindsay, K., Lipscomb, W. H., Mills, M. J., Neale, R., Oleson, K. W., Otto-Bliesner, B.,
 298 Phillips, A. S., Sacks, W., Tilmes, S., Kampenhout, L., Vertenstein, M., Bertini, A., Dennis, J., Deser, C.,
 299 Fischer, C., Fox-Kemper, B., Kay, J. E., Kinnison, D., Kushner, P. J., Larson, V. E., Long, M. C., Mickelson,
 300 S., Moore, J. K., Nienhouse, E., Polvani, L., Rasch, P. J., and Strand, W. G.: The Community Earth System
 301 Model Version 2 (CESM2), *J. Adv. Model. Earth Syst.*, 12, <https://doi.org/10.1029/2019MS001916>, 2020.

302 Del Negro, L. A., Fahey, D. W., Gao, R. S., Donnelly, S. G., Keim, E. R., Neuman, J. A., Cohen, R. C., Perkins, K. K.,
 303 Koch, L. C., Salawitch, R. J., Lloyd, S. A., Proffitt, M. H., Margitan, J. J., Stimpfle, R. M., Bonne, G. P., Voss,
 304 P. B., Wennberg, P. O., McElroy, C. T., Swartz, W. H., Kusterer, T. L., Anderson, D. E., Lait, L. R., and Bui,
 305 T. P.: Comparison of modeled and observed values of NO₂ and JNO₂ during the Photochemistry of Ozone Loss
 306 in the Arctic Region in Summer (POLARIS) mission, *J. Geophys. Res.*, 104, 26687–26703,
 307 <https://doi.org/10.1029/1999JD900246>, 1999.

308 Fabian, P., Pyle, J. A., and Wells, R. J.: Diurnal variations of minor constituents in the stratosphere modeled as a function
 309 of latitude and season, *J. Geophys. Res.*, 87, 4981, <https://doi.org/10.1029/JC087iC07p04981>, 1982.

310 Fischer, H., Birk, M., Blom, C., Carli, B., Carlotti, M., Endemann, M., Flaud, J. M., Gessner, R., Kleinert, A., Koopman,
 311 R., Langen, J., Lopez-Puertas, M., Mosner, P., Nett, H., Oelhaf, H., Perron, G., Remedios, J., Ridolfi, M., Stiller,
 312 G., and Zander, R.: MIPAS: an instrument for atmospheric and climate research, *Atmos. Chem. Phys.*,
 313 <https://doi.org/10.5194/acp-8-2151-2008>, 2008.

314 Funke, B., López-Puertas, M., von Clarmann, T., Stiller, G. P., Fischer, H., Glatthor, N., Grabowski, U., Höpfner, M.,
 315 Kellmann, S., Kiefer, M., Linden, A., Mengistu Tsidu, G., Milz, M., Steck, T., and Wang, D. Y.: Retrieval of
 316 stratospheric NOx from 5.3 and 6.2 μm nonlocal thermodynamic equilibrium emissions measured by Michelson
 317 Interferometer for Passive Atmospheric Sounding (MIPAS) on Envisat, *Journal of Geophysical Research:*
 318 *Atmospheres*, 110, <https://doi.org/10.1029/2004JD005225>, 2005.

319 Funke, B., García-Comas, M., Glatthor, N., Grabowski, U., Kellmann, S., Kiefer, M., Linden, A., López-Puertas, M.,
 320 Stiller, G. P., and von Clarmann, T.: Michelson Interferometer for Passive Atmospheric Sounding Institute of
 321 Meteorology and Climate Research/Instituto de Astrofísica de Andalucía version 8 retrieval of nitric oxide and
 322 lower-thermospheric temperature, *Atmos. Meas. Tech.*, 16, 2167–2196, [https://doi.org/10.5194/amt-16-2167-](https://doi.org/10.5194/amt-16-2167-2023)
 323 [2023](https://doi.org/10.5194/amt-16-2167-2023), 2023.

324 Gelaro, R., McCarty, W., Suárez, M. J., Todling, R., Molod, A., Takacs, L., Randles, C. A., Darmenov, A., Bosilovich, M.
 325 G., Reichle, R., Wargan, K., Coy, L., Cullather, R., Draper, C., Akella, S., Buchard, V., Conaty, A., da Silva,
 326 A. M., Gu, W., Kim, G.-K., Koster, R., Lucchesi, R., Merkova, D., Nielsen, J. E., Partyka, G., Pawson, S.,
 327 Putman, W., Rienecker, M., Schubert, S. D., Sienkiewicz, M., and Zhao, B.: The Modern-Era Retrospective
 328 Analysis for Research and Applications, Version 2 (MERRA-2), *J. Climate*, 30, 5419–5454,
 329 <https://doi.org/10.1175/JCLI-D-16-0758.1>, 2017.

330 Gettelman, A., Mills, M. J., Kinnison, D. E., Garcia, R. R., Smith, A. K., Marsh, D. R., Tilmes, S., Vitt, F., Bardeen, C. G.,
 331 McInerney, J., Liu, H. -L., Solomon, S. C., Polvani, L. M., Emmons, L. K., Lamarque, J. -F., Richter, J. H.,
 332 Glanville, A. S., Bacmeister, J. T., Phillips, A. S., Neale, R. B., Simpson, I. R., DuVivier, A. K., Hodzic, A.,
 333 and Randel, W. J.: The Whole Atmosphere Community Climate Model Version 6 (WACCM6), *JGR Atmos.*,
 334 124, 12380–12403, <https://doi.org/10.1029/2019JD030943>, 2019.

335 Johnston, H.: Reduction of Stratospheric Ozone by Nitrogen Oxide Catalysts from Supersonic Transport Exhaust, *Science*,
 336 173, 517–522, <https://doi.org/10.1126/science.173.3996.517>, 1971.

337 Johnston, H. S. and Podolske, J.: Interpretations of stratospheric photochemistry, *Rev. Geophys.*, 16, 491–519,
338 <https://doi.org/10.1029/RG016i004p00491>, 1978.

339 Junkermann, W., Platt, U., and Volz-Thomas, A.: A photoelectric detector for the measurement of photolysis frequencies
340 of ozone and other atmospheric molecules, *J. Atmos. Chem.*, 8, 203–227, <https://doi.org/10.1007/BF00051494>,
341 1989.

342 Kawa, S. R., Fahey, D. W., Solomon, S., Brune, W. H., Proffitt, M. H., Toohey, D. W., Anderson, D. E., Anderson, L. C.,
343 and Chan, K. R.: Interpretation of aircraft measurements of NO, ClO, and O₃ in the lower stratosphere, *J.*
344 *Geophys. Res.*, 95, 18597, <https://doi.org/10.1029/JD095iD11p18597>, 1990.

345 Kiefer, M., von Clarmann, T., Funke, B., García-Comas, M., Glatthor, N., Grabowski, U., Kellmann, S., Kleinert, A.,
346 Laeng, A., Linden, A., López-Puertas, M., Marsh, D. R., and Stiller, G. P.: IMK/IAA MIPAS temperature
347 retrieval version 8: nominal measurements, *Atmos. Meas. Tech.*, 14, 4111–4138, [https://doi.org/10.5194/amt-](https://doi.org/10.5194/amt-14-4111-2021)
348 [14-4111-2021](https://doi.org/10.5194/amt-14-4111-2021), 2021.

349 Kiefer, M., von Clarmann, T., Funke, B., García-Comas, M., Glatthor, N., Grabowski, U., Höpfner, M., Kellmann, S.,
350 Laeng, A., Linden, A., López-Puertas, M., and Stiller, G. P.: Version 8 IMK–IAA MIPAS ozone profiles:
351 nominal observation mode, *Atmos. Meas. Tech.*, 16, 1443–1460, <https://doi.org/10.5194/amt-16-1443-2023>,
352 2023.

353 Kinnison, D. E., Brasseur, G. P., Walters, S., Garcia, R. R., Marsh, D. R., Sassi, F., Harvey, V. L., Randall, C. E., Emmons,
354 L., Lamarque, J. F., Hess, P., Orlando, J. J., Tie, X. X., Randel, W., Pan, L. L., Gettelman, A., Granier, C.,
355 Diehl, T., Niemeier, U., and Simmons, A. J.: Sensitivity of chemical tracers to meteorological parameters in
356 the MOZART-3 chemical transport model, *J. Geophys. Res.*, 112, D20302,
357 <https://doi.org/10.1029/2006JD007879>, 2007.

358 Laepple, T., Schultz, M. G., Lamarque, J. F., Madronich, S., Shetter, R. E., Lefer, B. L., and Atlas, E.: Improved albedo
359 formulation for chemistry transport models based on satellite observations and assimilated snow data and its
360 impact on tropospheric photochemistry, *J. Geophys. Res.*, 110, D11308, <https://doi.org/10.1029/2004JD005463>,
361 2005.

362 Madronich, S.: Photodissociation in the atmosphere: I. Actinic flux and the effects of ground reflections and clouds, *J.*
363 *Geophys. Res.*, 92, 9740, <https://doi.org/10.1029/JD092iD08p09740>, 1987.

364 Madronich, S. and Weller, G.: Numerical integration errors in calculated tropospheric photodissociation rate coefficients,
365 *J Atmos Chem*, 10, 289–300, <https://doi.org/10.1007/BF00053864>, 1990.

366 Madronich, S., Hastie, D. R., Ridley, B. A., and Schiff, H. I.: Measurement of the photodissociation coefficient of NO₂ in
367 the atmosphere: I. Method and surface measurements, *J. Atmos. Chem.*, 1, 3–25,
368 <https://doi.org/10.1007/BF00113977>, 1983.

369 Madronich, S., Hastie, D. R., Schiff, H. I., and Ridley, B. A.: Measurement of the photodissociation coefficient of NO₂ in
370 the atmosphere: II, stratospheric measurements, *J. Atmos. Chem.*, 3, 233–245,
371 <https://doi.org/10.1007/BF00210498>, 1985.

372 Pommereau, J. P.: Observation of NO₂ diurnal variation in the stratosphere, *Geophys. Res. Lett.*, 9, 850–853,
373 <https://doi.org/10.1029/GL009i008p00850>, 1982.

374 Roscoe, H. K., Kerridge, B. J., Gray, L. J., Wells, R. J., and Pyle, J. A.: Simultaneous measurements of stratospheric NO
375 and NO₂ and their comparison with model predictions, *J. Geophys. Res.*, 91, 5405,
376 <https://doi.org/10.1029/JD091iD05p05405>, 1986.

377 Sagawa, H., Sato, T. O., Baron, P., Dupuy, E., Livesey, N., Urban, J., Von Clarmann, T., De Lange, A., Wetzzel, G., Connor,
378 B. J., Kagawa, A., Murtagh, D., and Kasai, Y.: Comparison of SMILES ClO profiles with satellite, balloon-
379 borne and ground-based measurements, *Atmos. Meas. Tech.*, 6, 3325–3347, [https://doi.org/10.5194/amt-6-](https://doi.org/10.5194/amt-6-3325-2013)
380 3325-2013, 2013.

381 Shao, Z.-D. and Ke, C.-Q.: Spring–summer albedo variations of Antarctic sea ice from 1982 to 2009, *Environ. Res. Lett.*,
382 10, 064001, <https://doi.org/10.1088/1748-9326/10/6/064001>, 2015.

383 Shetter, R., Junkermann, W., Swartz, W., Frost, G., Crawford, J., Lefer, B., Barrick, J., Hall, S., Hofzumahaus, A., Bais,
384 A., Calvert, J. G., Cantrell, C. A., Madronich, S., muller, M., Kraus, A., Monks, P. S., Edwards, G. D.,
385 McKenzie, R., Johnston, P., Schmitt, R., Griffioen, E., Krol, M., Kylling, A., Dickerson, R. R., Lloyd, S. A.,
386 Martin, T., Gardiner, B., Mayer, B., Pfister, E., Roth, E. P., keopke, P., Ruggaber, A., Schwander, H., and van
387 Weele, M.: Photolysis frequency of NO₂: measurement and modeling during the International Photolysis
388 Frequency Measurement and Modeling Intercomparison (IPMMI), *J. Geophys. Res.: Atmos.*, 108, 2003.

389 Shetter, R. E., McDaniel, A. H., Cantrell, C. A., Madronich, S., and Calvert, J. G.: Actinometer and Eppley radiometer
390 measurements of the NO₂ photolysis rate coefficient during the Mauna Loa Observatory photochemistry
391 experiment, *J. Geophys. Res.*, 97, 10349, <https://doi.org/10.1029/91JD02289>, 1992.

392 Solomon, S., Russell, J. M., and Gordley, L. L.: Observations of the diurnal variation of nitrogen dioxide in the stratosphere,
393 *J. Geophys. Res.*, 91, 5455, <https://doi.org/10.1029/JD091iD05p05455>, 1986.

394 Von Clarmann, T., Höpfner, M., Kellmann, S., Linden, A., Chauhan, S., Funke, B., Grabowski, U., Glatthor, N., Kiefer,
395 M., and Schieferdecker, T.: Retrieval of temperature, H₂O, O₃, HNO₃, CH₄, N₂O, ClONO₂ and ClO from
396 MIPAS reduced resolution nominal mode limb emission measurements, *Atmospheric Measurement*
397 *Techniques*, 2, 159–175, <https://doi.org/10.5194/amt-2-159-2009>, 2009.

398 Webster, C. R. and May, R. D.: Simultaneous in situ measurements and diurnal variations of NO, NO₂, O₃, j NO₂, CH₄,
399 H₂O, and CO₂ in the 40- to 26-km region using an open path tunable diode laser spectrometer, *J. Geophys. Res.*,
400 92, 11931, <https://doi.org/10.1029/JD092iD10p11931>, 1987.

401